Objective quasicontinuum approach for rod problems

Ye. Hakobyan,[*] E. B. Tadmor,[†] and R. D. James[‡]
Department of Aerospace Engineering and Mechanics, University of Minnesota, Minneapolis, Minnesota 55455, USA
(Received 6 September 2012; published 28 December 2012)

An objective quasicontinuum (OQC) method is developed for simulating rodlike systems that can be represented as a combination of locally objective structures. An objective structure (OS) is one for which a group of atoms, called a "fundamental domain" (FD), is repeated using specific rules of translation and rotation to build a more complex structure. An objective Cauchy-Born rule defines the kinematics of the OS atoms in terms of a set of symmetry parameters and the positions of the FD atoms. The computational advantage lies in the capability of representing a large system of atoms through a small set of symmetry parameters and FD atom positions. As an illustrative example, we consider the deformation of a copper single-crystal nanobeam which can be described as an OS. OQC simulations are performed for uniform and nonuniform bending for two different orientations (nanobeam axis oriented along [111] and [100]) and compared with elastica results. In the uniform bending case, the [111]-oriented single-crystal nanobeam experiences elongation, while the [100]-oriented nanobeam experiences contraction in total length. The nonuniform bending allows for stretching, contraction, and bending as deformation. Under certain loading conditions, dislocation nucleation is observed within the FD.

DOI: 10.1103/PhysRevB.86.245435 PACS number(s): 61.46.Km, 62.23.Hj, 81.07.Gf, 02.70.Ns

I. INTRODUCTION

A rodlike structure is a three-dimensional structure that satisfies certain geometric constraints such as having two of its dimensions smaller in magnitude relative to the third or forming a material curve with finite thickness bounded by its lateral surface. The analysis of deformations of rods is of considerable importance due to recent interest in the mechanical properties of nanoscale rodlike structures ranging from nanotubes to polymer chains and DNA strands. For example, the mechanical properties of some nanorods exhibit considerably greater strength than those that are observed in macroscopic single crystals,[1] suggesting new composite materials. Special attention is given to experimental results pertaining to nanotubes[1–3] and nanobeams.[1,4,5] Due to their unique physical properties, nanobeams are considered to be important building blocks for studies of the physical properties of nanoscale structures and the assembly of a wide range of functional nanometer-scale systems.[6,7]

The analysis of the mechanical properties of nanoscale rodlike structures divides into two main approaches. In the first, the results of the continuum theory of elasticity are used to obtain surface and edge corrections for nanoscale effects (see, for example, Refs. 8 and 9). The second approach involves the extraction of the overall response from the underlying atomic interactions (refer to Ref. 10). The conditions under which continuum theories of bulk systems can be applied to nanoscale objects remain an area of open research.

We suggest approaching this challenge through the quasicontinuum (QC) method, which was originally developed for simple crystal materials[11,12] and later extended to multilattices.[13] In the local limit of QC, every point in a continuum corresponds to an infinite periodic region on the atomistic scale. The constitutive response of the system is obtained from an atomistic computation through application of the Cauchy-Born rule rather than an empirical phenomenological relation. In this paper, we extend the local QC method to objective structures. The resulting *objective quasicontinuum* (OQC) method is used for simulating systems that are not objective but can be represented as a combination of locally objective structures. (Objective structures are defined in Sec. II.)

The OQC formulation is inspired by a Cosserat point approach for nonlinear rods with rigid cross sections of Rubin and co-workers.[14,15] Similar to the Cosserat point approach, the constitutive relations are the key to making the connection between the continuum OQC formulation and objective structures. Assuming a conservative system, constitutive relations can be derived by relating resultant forces and couples to derivatives of a strain energy function. In OQC, the strain energy function is computed from an objective molecular statics calculation by analogy to the method described in Ref. 16. OQC has two major benefits: (1) It is computationally efficient. Through the introduction of local objective structures, the large numbers of atoms making up a nanorod are represented by a small set of symmetry parameters and fundamental domain atoms. (2) The local constitutive relations for the rod are obtained from first principles as opposed to phenomenological models. The results of an OQC simulation are therefore predictive.

As a practical example, OQC is applied to study the uniform and nonuniform bending of single-crystal copper nanobeams which can be described as objective structures (see Sec. II A).

II. OBJECTIVE STRUCTURES

An *objective structure*[17] (OS) is one for which a finite unit of atoms, called a "fundamental domain" (FD), is repeated using specific rules of translation and rotation to build a more complex structure. The images of the FD generated by this replication rule are called "molecules." The result is a generalization of crystal structures to structures for which the corresponding atoms in each molecule experience identical environments up to an orthogonal transformation and

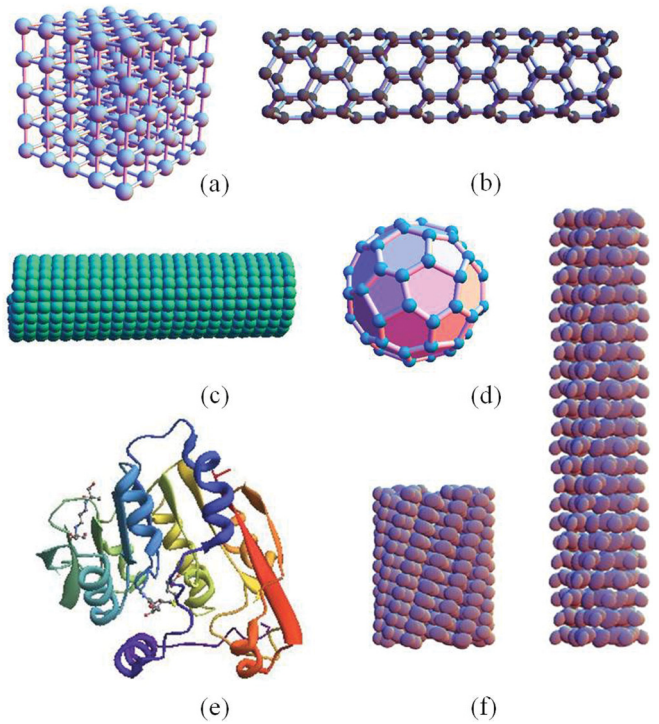

FIG. 1. (Color online) Examples of OSs include (a) crystals, (b) nanotubes, (c) viral capsids, (d) buckyballs, (e) common proteins, and (f) contracted and extended tail sheaths of bacteriophage T4.

translation. More precisely, a set of position vectors

$$\mathrm{OS} = \{\mathbf{x}_{J,k} : J = 1,\ldots,N, k = 1,\ldots,M\}, \tag{1}$$

where J denotes the molecule and k enumerates atoms within it, is an OS, if there exist NM orthogonal matrices $\{\mathbf{Q}_{1,1},\ldots,\mathbf{Q}_{N,M}\}$ such that

$$\mathrm{OS} = \{\mathbf{x}_{J,k} + \mathbf{Q}_{J,k}(\mathbf{x}_{I,m} - \mathbf{x}_{1,k}) : I = 1,\ldots,N, m = 1,\ldots,M\} \tag{2}$$

for every $J \in \{1,\ldots,N\}$ and $k \in \{1,\ldots,M\}$.

Many of the most actively studied structures in science are OSs (Fig. 1), including crystals, nanobeams and nanowires, carbon nanotubes, C60, many of the common proteins (hemoglobin, actin, collagen), viral capsids and parts (baseplates, tails, necks), various kinds of molecular fibers, bilayers (staggered and unstaggered), and others.[17] In this paper, we focus on rodlike structures (nanobeams, nanowires, nanotubes, viral parts, and various kinds of molecular fibers).

By definition, the isometry group G of an objective structure OS (or any structure) is the set of all orthogonal transformations and translations, usually written $(\mathbf{Q}|\mathbf{c}) \in G$, that preserve the structure, that is, that satisfy

$$\mathbf{Q}\mathbf{x}_{J,\ell} + \mathbf{c} = \mathbf{x}_{\Pi(J,\ell)}, \quad J = 1,\ldots,N, \quad \ell = 1,\ldots,M \tag{3}$$

for some permutation Π. In cases that one assigns a species to atom J,ℓ, then Π is required to preserve the species, that is, if $K,m = \Pi(J,\ell)$, then atom K,m is the same species as atom J,ℓ. These transformations form a group under the product $(\mathbf{Q}_1|\mathbf{c}_1)(\mathbf{Q}_2|\mathbf{c}_2) = (\mathbf{Q}_1\mathbf{Q}_2|\mathbf{c}_1 + \mathbf{Q}_1\mathbf{c}_2)$ and with $(\mathbf{I}|0)$ being the identity.

Each OS can be constructed as the orbit of an isometry group on molecule 1, $\mathcal{M}_1 = \{\mathbf{x}_{1,k}, k = 1,\ldots,M\}$. To see this, rearrange the definition of an OS as $\mathbf{Q}_{J,k}\mathbf{x}_{I,m} + \mathbf{x}_{J,k} - \mathbf{Q}_{J,k}\mathbf{x}_{1,k} = \mathbf{x}_{\Pi(I,m)}$. Thus, $(\mathbf{Q}_{J,k}|\mathbf{x}_{J,k} - \mathbf{Q}_{J,k}\mathbf{x}_{1,k})$ belongs to the isometry group G of the OS for each J,k. Now note that, trivially, $\mathbf{x}_{J,k} = \mathbf{Q}_{J,k}\mathbf{x}_{1,k} + \mathbf{x}_{J,k} - \mathbf{Q}_{J,k}\mathbf{x}_{1,k} = \mathbf{Q}\mathbf{x}_{1,k} + \mathbf{c}$, where $(\mathbf{Q}|\mathbf{c}) = (\mathbf{Q}_{J,k}|\mathbf{x}_{J,k} - \mathbf{Q}_{J,k}\mathbf{x}_{1,k}) \in G$, by the above. Thus, the OS is contained in the orbit of $\mathcal{M}_1$ under G. Conversely, putting $j = 1$ in (3) we get that the orbit of $\mathcal{M}_1$ under G is contained in the OS, completing the argument.

A *fundamental domain* of an isometry group, denoted FD, is a set in $\mathbb{R}^3$ with the property that images of the FD under the group are nonoverlapping and fill $\mathbb{R}^3$. Any collection of atoms in the FD can serve as a molecule, and conversely, the intersection of any OS with its FD can be taken as molecule 1. This terminology is used below.

A. Objective structures for rod deformations

A rodlike structure such as a nanobeam can be described as an OS where the FD is a "slice" of the beam. For example, Fig. 2 shows various nanobeams that are generated by a planar array of atoms [Fig. 2(a)] lying in an FD of various groups. All of these beams are obtained by using the basic helical group $G = \{[\mathbf{Q}|\lambda\mathbf{e} + (\mathbf{I} - \mathbf{Q})\mathbf{x}_0]^J : J \in \mathbb{Z}\} = \{[\mathbf{Q}^J|J\lambda\mathbf{e} + (\mathbf{I} - \mathbf{Q}^J)\mathbf{x}_0] : J \in \mathbb{Z}\}$ in the notation introduced above, where $\mathbf{Q}$ is a rotation matrix and the unit vector $\mathbf{e}$ defines its axis $\mathbf{Q}\mathbf{e} = \mathbf{e}$. This group consists of powers of the basic isometry $g = [\mathbf{Q}|\lambda\mathbf{e} + (\mathbf{I} - \mathbf{Q})\mathbf{x}_0]$, called a screw transformation, which represents a rotation about the axis $\mathbf{e}$ passing through the fixed point $\mathbf{x}_0$, followed by a translation of amount λ in the direction $\mathbf{e}$. The beam is generated by applying G to a slice, represented by $\mathbf{x}_{\mathrm{FD},k}$, $k = 1,\ldots,M$, that is,

$$\mathbf{x}_{J,k} = g^J(\mathbf{x}_{\mathrm{FD},k}) = \mathbf{Q}^J\mathbf{x}_{\mathrm{FD},k} + J\lambda\mathbf{e} + (\mathbf{I} - \mathbf{Q}^J)\mathbf{x}_0. \tag{4}$$

For example, referring to the orthonormal basis shown in Fig. 2, various deformations can be obtained by fixing the

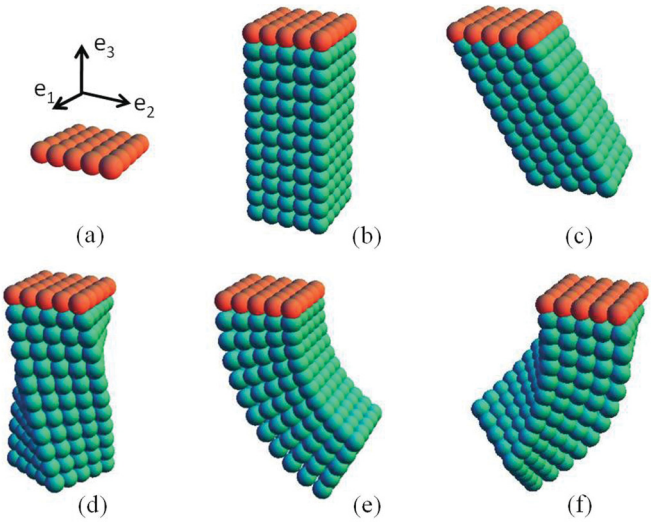

FIG. 2. (Color online) Deformations in a nanobeam: (a) a molecule or FD, (b) axial stretch/compression, (c) simple shear, (d) pure torsion, (e) pure bending, and (f) torsion-bending combination.

atoms in the slice $\mathbf{x}_{\mathrm{FD},k}$, $k = 1, \ldots, M$ and applying the formula above with suitable choices of the parameters. A simple extension with axial stretch $\lambda \neq 0$ is obtained by using the choices $\mathbf{Q} = \mathbf{I}, \mathbf{e} = \mathbf{e}_3$ [see Fig. 2(b)]. A shear [Fig. 2(c)] is obtained similarly by choosing $\lambda \neq 0$ and $\mathbf{e} \cdot \mathbf{e}_3 \neq 0, 1$. A torsional deformation [Fig. 2(d)] is given by the choices $\mathbf{Q} \neq \mathbf{I}$, $\mathbf{e} \parallel \mathbf{e}_3$, $\lambda \neq 0$, $\mathbf{x}_0 = 0$. A pure bending deformation as shown in Fig. 2(e) results by choosing $\mathbf{Q} \neq \mathbf{I}$, $\mathbf{e} \parallel \mathbf{e}_1$, $\lambda = 0$, $\mathbf{x}_0 = \delta \mathbf{e}_2$, for a suitable $\delta > 0$. Finally, a general helical deformation as seen in Fig. 2(f) is given by generic choices of the parameters.

Note, that all of the above structures are objective, irrespective of the choice of atoms in the FD or the values of the symmetry parameters λ, $\mathbf{x}_0$ and the angles of rotation in $\mathbf{Q}$. For equilibrium structures, the symmetry parameters and the positions of atoms in the FD are determined by the applied loading and the interatomic forces.

III. MULTISCALE MODELING USING THE OBJECTIVE QUASICONTINUUM APPROACH

Methods for performing molecular dynamics and molecular statics on OSs are described in Ref. 16. Such *objective molecular statics* (OMS) simulations are limited to perfect OSs. It is possible to use OMS to simulate the uniform bending or twisting of an infinite nanobeam or carbon nanotube. However, nonuniform bending of a nanobeam, where the curvature varies along the length of the beam, is not possible. Another difficulty arises if the structure is finite or contains a defect of some sort. In this case, it is no longer a perfect OS and can not be modeled by OMS. As an alternative, in OQC we propose to model such structures by approximating the energy at each point in the structure using an energy density computed from a locally objective structure.

As mentioned in the Introduction, constitutive equations are the key to making the connection between the atomic level and the continuum. Constitutive equations which are used in rod theories to couple the geometry of the rodlike structure and the material properties introduce constraints on the deformation of the rod (linear or nonlinear) and assume a form of material response (elastic or nonelastic) (see, for example, Refs. 18–23). A classical example of a constrained rod theory is the *elastica* rod of Kirchhoff and Euler,[18] with rigid cross sections that remain normal to an inextensible reference curve. We will use elastica theory below for comparison with our results. In the OQC approach proposed here, instead of introducing *a priori* constraints on the constitutive response, it emerges naturally as an output of the atomic interactions.

IV. OBJECTIVE QUASICONTINUUM

The OQC formulation is inspired by the theory of a *Cosserat point* originally introduced by Rubin and co-workers.[14,15,23–25] This theory can be used to obtain numerical solutions for the dynamical motion of nonlinear rods. Following the usual finite element methodology, the rod is divided into N elements, where each element is a structure modeled as a Cosserat point. An element is bounded by a lateral surface and two end cross sections. The Ith cross section can be described by the location

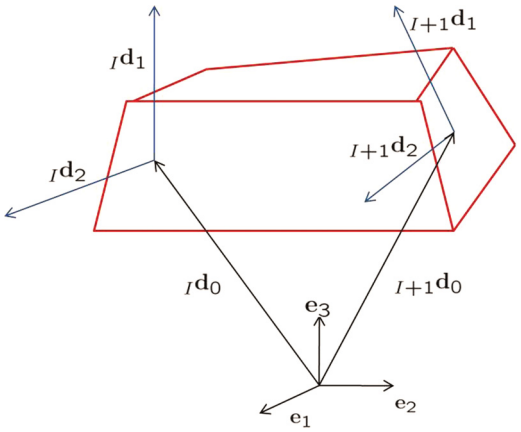

FIG. 3. (Color online) Cosserat rod element.

of the centroid $_I\mathbf{d}_0$ and two vectors $\{_I\mathbf{d}_1, _I\mathbf{d}_2\}$ lying within the cross section (see Fig. 3). This gives 9 degrees of freedom for each cross section for a total of 18 degrees of freedom per element. A simplified theory is obtained by assuming that the cross sections are rigid as done by Brand and Rubin.[15] In this case, the unit vectors $\{_I\mathbf{d}_1, _I\mathbf{d}_2\}$ are perpendicular to each other (as in Fig. 3), thereby reducing the number of degrees of freedom to 12 per element.

The constitutive response for a Cosserat point element is obtained by postulating a nonlinear phenomenological form in terms of the element degrees of freedom and fitting the parameters in this form to analytic results from small strain elasticity theory.[15,23] This is different from finite element formulations for bulk materials where a strain energy density function characterizes the material response, and the element response then follows by integration.

OQC differs from the Cosserat point approach in two main aspects. First, the kinematics of the element is different since now each element is associated with an OS (rather than the general structure depicted in Fig. 3). Thus, instead of the 18 (or 12) kinematic degrees of freedom characterizing the Cosserat point element, an OQC element is characterized by the symmetry parameters of the OS and the positions of the FD atoms. Second, instead of the phenomenological constitutive model of the Cosserat point element, the constitutive response of an OQC element is obtained by performing an OMS calculation on the FD atoms with appropriate objective boundary conditions.

The total energy of an OQC model divided into N elements is

$$E_{\mathrm{OQC}} = \sum_{i=1}^{N} E_{\mathrm{el}}^{(i)}, \tag{5}$$

where $E_{\mathrm{el}}^{(i)}$, the energy of the ith element, is given by

$$E_{\mathrm{el}}^{(i)} = n_{\mathrm{FD}}^{(i)} E_{\mathrm{FD}}^{(i)}. \tag{6}$$

Here, $n_{\mathrm{FD}}^{(i)}$ is the number of images of the FD (number of molecules) within element i and $E_{\mathrm{FD}}^{(i)}$ is the energy of the FD associated with it. The FD energy will depend on the symmetry parameters of element i (determined from its nodal values) and the positions of the FD atoms which constitute internal

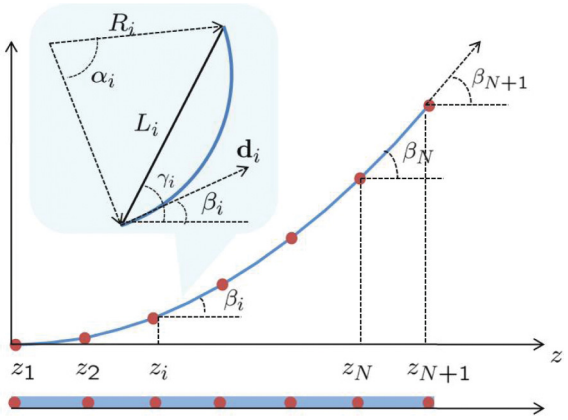

FIG. 4. (Color online) 1D OQC model consisting of N elements.

element variables. This is analogous to the Cauchy-Born rule for multilattice crystals[13] and can therefore be referred to as the *objective Cauchy-Born rule*.

A. OQC kinematics

In order to demonstrate the OQC methodology, we consider the nonuniform bending of a one-dimensional (1D) rodlike structure. The rod is divided into N elements delimited by $N+1$ nodes. Each node is characterized by its position z_i ($i = 1,\ldots,N+1$) along the horizontal z axis, and the angle β_i between the tangent to the rod at the position of the node $\mathbf{d}_i = (\sin\beta_i, 0, \cos\beta_i)$ and the horizon (see Fig. 4). Next, we limit the kinematics of an element to that of an arc of constant radius (so that a locally objective structure is retained). The arc is characterized by the symmetry parameters α_i and R_i (see inset in Fig. 4):

$$\alpha_i = \beta_{i+1} - \beta_i, \quad R_i = \frac{L_i}{2\sin(\alpha_i/2)}, \tag{7}$$

where

$$L_i = \frac{z_{i+1} - z_i}{\cos\gamma_i}, \quad \gamma_i = \frac{\beta_{i+1} + \beta_i}{2}. \tag{8}$$

While the angle α_i and the radius of curvature R_i are natural parameters with which to describe arc-shaped elements, the variables γ_i and L_i are preferable to work with in practice since R_i tends to infinity when the beam is flat, which leads to numerical difficulties. In the case of a torsion-bending combination, the torsion angle within an element needs to be added.

Modeling each element as a circular arc with a different curvature radius is an approximation similar to the finite element method in 1D with constant strain elements. In both cases, one can approach a nonuniform deformation as closely as one likes as the element size becomes infinitely small.

B. OQC element constitutive model

The energy of an OQC element given in Eq. (6) is a multiple of the energy of the FD, E_{FD}, of the OS associated with the element. This energy is a function of the symmetry parameters defining the OS (see Sec. IV A) and the positions of the FD atoms. It is computed via OMS by constructing the FD in a computer with the necessary neighbors generated by the application of objective boundary conditions.

The kinematics of the rod OS is described in Sec. IV A. For constructing the FD images, it is convenient to work with the element angle α and length L [see Eqs. (7) and (8)]. Since the FD energy is rotationally invariant, we can simply set the tangent vector to $\mathbf{d} = (0,0,1)$. Note that for notational simplicity, we omit the element index i, taking all element quantities to refer to a generic element.

For any atom $\mathbf{x}_{\mathrm{FD,k}}$ ($k = 1,\ldots,M$) within the FD, the image in the Jth molecule is

$$\mathbf{x}_{J,k} = \mathbf{x}_c + \mathbf{Q}\left(\frac{\alpha J}{n_{\mathrm{FD}}}\right)\cdot(\mathbf{x}_{\mathrm{FD,k}} - \mathbf{x}_{\mathbf{c}}) + l_J\mathbf{Q}\left(\frac{\alpha J}{2n_{\mathrm{FD}}}\right)\cdot\mathbf{d}, \tag{9}$$

where $\mathbf{Q}(\theta)$ is a counterclockwise rotation by angle θ around the axis perpendicular to the plane containing the rod, $\mathbf{x}_c$ is the center of mass of the FD, and l_J is the distance between $\mathbf{x}_c$ and its position in the Jth image (see Fig. 5):

$$\mathbf{x}_c = \frac{\sum_{k=1}^{M} m_k\mathbf{x}_{\mathrm{FD,k}}}{\sum_{k=1}^{M} m_k} \quad \text{and} \quad l_J = L\frac{\sin\frac{\alpha J}{2n_{\mathrm{FD}}}}{\sin\frac{\alpha}{2}}, \tag{10}$$

where m_k is the mass of the kth atom. Equation (9) describes the general case of bending and extension. Setting $\alpha = 0$, Eq. (9) reduces to the following simpler expression for the special case of axial stretching and compression:

$$\mathbf{x}_{J,k} = \mathbf{x}_{\mathrm{FD,k}} + l_J\mathbf{d}. \tag{11}$$

The energy of the FD and the forces on the FD atoms are computed from an interatomic model. In the case of pair potential interactions (Lennard-Jones potential for example), the energy of the FD is

$$\begin{aligned} E_{\mathrm{FD}} &= \frac{1}{2}\sum_{i\in\mathrm{FD}}\sum_{\substack{j\in\mathrm{FD}\\ j\neq i}}\phi_{ij}(r_{ij}) + \frac{1}{2}\sum_{i\in\mathrm{FD}}\sum_{j\notin\mathrm{FD}}\phi_{ij}(r_{ij}) \\ &= \frac{1}{2}\sum_{i\in\mathrm{FD}}\sum_{\substack{j\\ j\neq i}}\phi_{ij}(r_{ij}), \end{aligned} \tag{12}$$

where r_{ij} is a distance between atoms i and j, $r_{ij} < r_{\mathrm{cut}}$ (the cutoff radius of the interaction potential). Note that for atoms $j \notin$ FD, the position is determined through the atoms in the FD $\mathbf{x}_{\mathrm{FD,k}}$ and symmetry parameters through Eq. (9). Thus, to compute the energy of the FD correctly, it is necessary to construct n_{img} image layers on both sides of the FD to ensure that every atom in the FD has all of its neighbors up to the cutoff distance r_{cut} [see Fig. 6(a)]. In a numerical implementation, the padding around the FD atoms is increased to $r_{\mathrm{cut}} + \delta$ (where δ is a fraction of the cutoff radius, typically about 20%). This prevents the need to recompute the neighbors of the FD atoms at each minimization step (as described in the next section) and therefore reduces the computational cost (see, for example, Ref. 26).

In the numerical examples presented in Sec. V, an embedded atom method (EAM) potential[27] suitable for describing metals was used. For an EAM potential, the energy of the FD

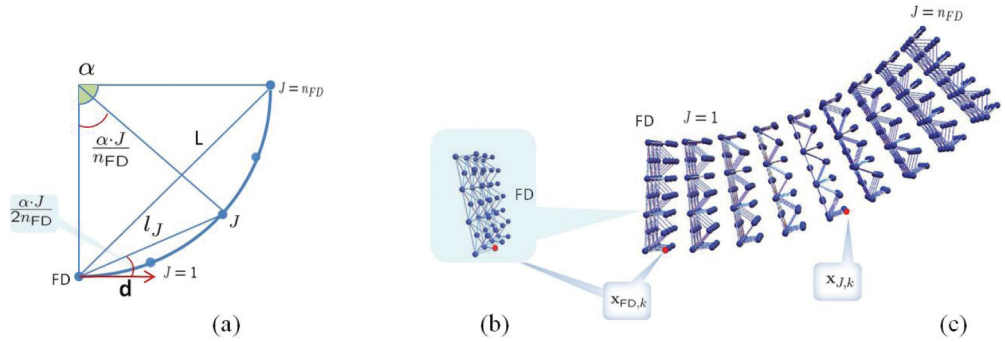

FIG. 5. (Color online) (a) Geometry of an OQC element, (b) fundamental domain, (c) OS generated by replicating the FD.

is

$$E_{\mathrm{FD}} = \frac{1}{2}\sum_{i\in\mathrm{FD}}\sum_{\substack{j\\ j\neq i}}\phi_{ij}(r_{ij}) + \sum_{i\in\mathrm{FD}} U_i(\rho_i),$$
$$\rho_i = \sum_{\substack{j\\ j\neq i}} g_j(r_{ij}), \tag{13}$$

where $r_{ij} < r_{\mathrm{cut}}$, ϕ_{ij} is a pair potential function, $g_j(r_{ij})$ is the contribution to the electron charge density at the position of atom i due to atom j, and U_i is an embedding function representing the energy required to place atom i into the electron density ρ_i at its location.

C. OQC energy minimization

The total energy of an OQC system is given in Eq. (5). This energy depends on the nodal degrees of freedom z_i and β_i $(i = 1, N+1)$ and the positions of the FD atoms associated with each element $\mathbf{x}^{(i)}_{\mathrm{FD,k}}$ $(i = 1,\ldots,N)$. This constitutes a set of $2(N+1)+3MN$ global degrees of freedom for the OQC formulation.

To find the equilibrium of the system, we also need to take into account the potential $-W(z_1,\beta_1,\ldots,z_{N+1},\beta_{N+1})$ of the external forces or moments. The potential energy functional of the system is

$$\Pi = E_{\mathrm{OQC}} - W = \Pi\left(z_1,\beta_1,\ldots,z_{N+1},\beta_{N+1},\left\{\mathbf{x}^{(i)}_{\mathrm{FD,k}}\right\}_{i=1,\ldots,N,k=1,\ldots,M}\right). \tag{14}$$

The potential of the external loads $-W$ depends on the loading conditions. For example, for a cantilever nanobeam subjected to an upward point force $\mathcal{F}$ applied at its free end (node $N+1$):

$$\Pi = \sum_{i=1}^{N} n^{(i)}_{\mathrm{FD}} E^{(i)}_{\mathrm{FD}} - \mathcal{F}\sum_{i=1}^{N}(z_{i+1}-z_i)\tan\left(\frac{\beta_{i+1}+\beta_i}{2}\right), \tag{15}$$

with $z_1 = 0, \beta_1 = 0$ at the fixed end as the boundary conditions. If instead of a point load, a pure moment $\mathcal{M}$ is applied at its free end, the appropriate potential energy is

$$\Pi = \sum_{i=1}^{N} n^{(i)}_{\mathrm{FD}} E^{(i)}_{\mathrm{FD}} - \mathcal{M}\beta_{N+1}. \tag{16}$$

To minimize the total potential energy, we use the nonlinear conjugate gradient (CG) method, in which, in addition to the functional in Eq. (14), we need to supply the gradient (derivatives of the potential energy with respect to all independent variables). Using Eqs. (14) and (5), we have

$$\frac{\partial\Pi}{\partial\mathbf{x}^{(i)}_{\mathrm{FD,k}}} = -n^{(i)}_{\mathrm{FD}}\mathbf{f}^{(i)}_{\mathrm{FD,k}} = n^{(i)}_{\mathrm{FD}}\frac{\partial E^{(i)}_{\mathrm{FD}}}{\partial\mathbf{x}^{(i)}_{\mathrm{FD,k}}}. \tag{17}$$

In nonobjective atomistic simulations, $\mathbf{f}^{(i)}_{\mathrm{FD,k}}$ can always[28] be represented as a pairwise sum of forces due to neighboring atoms within some finite distance (r_{cut} for a pair potential and $2r_{\mathrm{cut}}$ for EAM). However, with objective boundary conditions, there is an additional contribution to the force since the interaction between a pair of atoms contributes to the forces on all other atoms in the FD due to Eq. (9). It is easy to show that in the case of a pure moment applied at the free end [see Eq. (16)], this additional term equals zero. More details on derivation of the force in Eq. (17) for pair potential and EAM interactions are presented in the Appendix.

Similarly, we need to provide derivatives of Π with respect to z_i and β_i $(i = 1,\ldots,N)$. Since the energy of the FD also depends on the symmetry parameters α and L in each element, it is necessary to use the chain rule to compute derivatives with respect to z_i and β_i. Each element has nodal values $z_{(1)}$, $\beta_{(1)}$, $z_{(2)}$, $\beta_{(2)}$ (local numbering). Therefore,

$$\frac{\partial E_{\mathrm{FD}}}{\partial\beta_{(i)}} = \sum_{j\notin\mathrm{FD}}\frac{\partial E_{\mathrm{FD}}}{\partial\mathbf{x}_j}\left(\frac{\partial\mathbf{x}_j}{\partial L}\frac{\partial L}{\partial\beta_{(i)}} + \frac{\partial\mathbf{x}_j}{\partial\alpha}\frac{\partial\alpha}{\partial\beta_{(i)}}\right) \tag{18}$$

and

$$\frac{\partial E_{\mathrm{FD}}}{\partial z_{(i)}} = \sum_{j\notin\mathrm{FD}}\frac{\partial E_{\mathrm{FD}}}{\partial\mathbf{x}_j}\frac{\partial\mathbf{x}_j}{\partial L}\frac{\partial L}{\partial z_{(i)}}, \tag{19}$$

where

$$\alpha = \beta_{(2)} - \beta_{(1)} \quad \text{and} \quad \mathrm{L} = \frac{\mathrm{z}_{(2)} - \mathrm{z}_{(1)}}{\cos\frac{\beta_{(2)}+\beta_{(1)}}{2}}. \tag{20}$$

Finally, we need to add derivatives over global variables coming from the potential of the external forces or moments when applied [see, for example, Eqs. (15) and (16)]. Thus, going back to global numeration, we have

$$\frac{\partial\Pi}{\partial z_i} = n^{(i)}_{\mathrm{FD}}\frac{\partial E^{(i)}_{\mathrm{FD}}}{\partial z_i} + n^{(i-1)}_{\mathrm{FD}}\frac{\partial E^{(i-1)}_{\mathrm{FD}}}{\partial z_i} - \frac{\partial W}{\partial z_i} \tag{21}$$

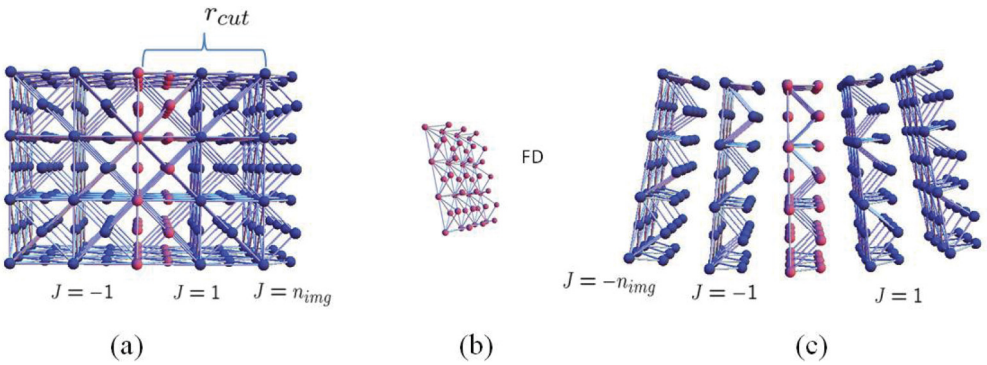

FIG. 6. (Color online) (a) FD with image layers for periodic boundary conditions, (b) FD example, (c) FD with image layers for objective boundary conditions.

and

$$\frac{\partial \Pi}{\partial \beta_i} = n_{\mathrm{FD}}^{(i)} \frac{\partial E_{\mathrm{FD}}^{(i)}}{\partial \beta_i} + n_{\mathrm{FD}}^{(i-1)} \frac{\partial E_{\mathrm{FD}}^{(i-1)}}{\partial \beta_i} - \frac{\partial W}{\partial \beta_i}. \tag{22}$$

V. EXAMPLES

In this section, we present the results of OQC calculations for nanobeams under different loading conditions. The OQC results are compared with elastica where possible. Failure within the FD due to dislocation nucleation is also explored. The section concludes with an error analysis of the OQC method.

A. Cantilever nanobeams with a point load at the free end

Consider a face-centered-cubic (fcc) single-crystal copper nanobeam of length 1735.2 Å with a square cross section of size 86.76 Å, i.e., with a side-to-length ratio of 1:20. An EAM model[29] is used to describe the atomic interactions in the copper. The nanobeam is oriented with its [100]-crystallographic direction along the z axis [see Figs. 7(a) and 7(b)] with $L_0 = 480a_0$ and $H = W = 24a_0$, where $a_0 = 3.615$ Å is the lattice constant of bulk fcc copper.

This system, when fully simulated, consists of 1 152 480 atoms corresponding to 3 457 440 degrees of freedom. It is modeled using OQC with 3 or 6 elements with a FD of 2401

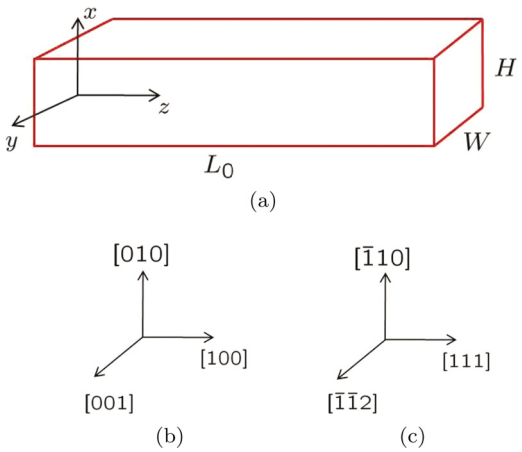

FIG. 7. (Color online) (a) Schematic of the nanobeam, (b) [100] nanobeam, (c) [111] nanobeam.

atoms for a total of 21 617 or 43 232 degrees of freedom. The nanobeam is fixed at the left end and loaded by an upward point force $\mathcal{F}$ at its free end on the right. We therefore minimize the potential energy in Eq. (15) for a given value of $\mathcal{F}$. In all simulations, a uniform mesh is used (i.e., all elements are the same size) with the same FDs.

The simulations are performed as follows:

(1) The FD is constructed for the appropriate orientation of the fcc copper crystal with sufficient images [see Fig. 5(b)] to enable calculation of the energy and forces on the FD atoms.

(2) The FD energy is minimized with respect to the FD atom positions. This causes the FD to distort slightly due to surface effects. (The FD exhibits a contraction in length of about 0.59% in this particular case.)

(3) The OQC model is set up. The initial positions of the FD atoms within each element are set to the relaxed FD structure. The nodal values are initialized.

(4) Boundary conditions are applied. For the present simulation, a force $\mathcal{F}$ in the x direction (vertical direction) is applied at the free end node $(N+1)$. The left end of the beam is fixed with $z_1 = 0$ and $\beta_1 = 0$.

(5) The equilibrium configuration of the system is computed for each value of the force $\mathcal{F}$. The force $\mathcal{F}$ is then increased by a small increment $\Delta\mathcal{F} = 0.02$ eV/Å and the previous solution is used as the initial guess for the next step in the computation.

The results of the OQC simulations are compared with continuum elastica solutions.[18,30] The cross section of the nanobeam is relatively large on the atomic scale and therefore surface effects can be neglected.[8,9] This means that the standard bulk definition of Young's modulus without the surface effect corrections may be used in the elastica solution. The directional Young's moduli for the crystallographic orientations being considered here are[31]

$$\begin{aligned} Y_{[100]} &= \frac{(c_{11}+2c_{12})(c_{11}-c_{12})}{c_{11}+c_{12}}, \\ Y_{[111]} &= \frac{3c_{44}(c_{11}+2c_{12})}{c_{11}+2c_{12}+c_{44}}, \end{aligned} \tag{23}$$

where c_{11}, c_{12}, and c_{44} are the cubic elastic constants of the copper single crystal. For the EAM model[29] used here, these are $c_{11} = 1.042\,33$ eV/Å^3, $c_{12} = 0.773\,95$ eV/Å^3, and $c_{44} = 0.474\,36$ eV/Å^3, from which $Y_{[100]} = 0.382\,74$ eV/Å^3 and $Y_{[111]} = 1.202\,78$ eV/Å^3.

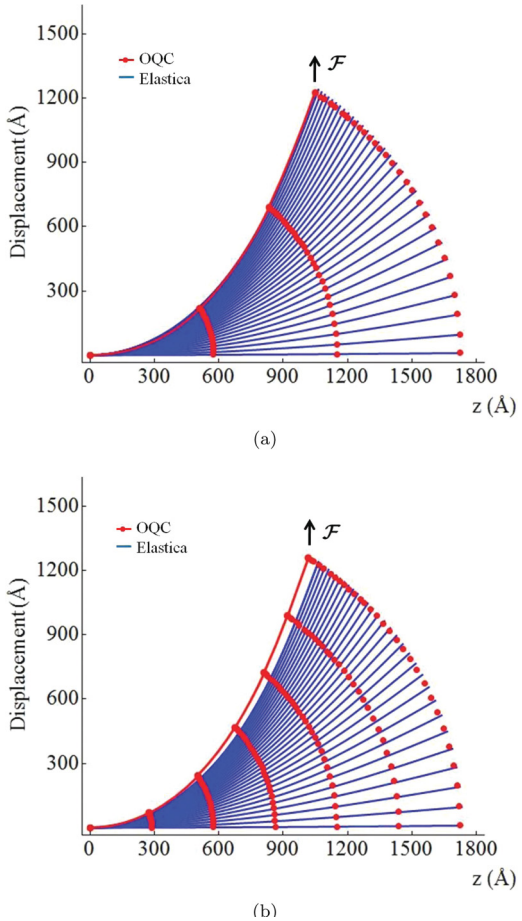

FIG. 8. (Color online) OQC results for nonuniform bending of a single-crystal copper nanobeam with square cross section, oriented in the [100] direction. (a) 3-element model, (b) 6-element model. OQC results (red lines and dots) are compared with elastica solutions shown as blue lines.

Figure 8 presents the results of the OQC simulations (red) and the elastica solutions (blue) for the [100] single-crystal copper nanobeam with fixed left end and a point upward force $\mathcal{F}$ applied to the free end. The red dots correspond to the OQC node positions and the lines between them are the circular arcs defined by the symmetry parameters. Results are shown every five load steps, i.e., for force values of $\mathcal{F} = 0$, 0.1 eV/Å, 0.2 eV/Å, and so on. The largest value shown is $\mathcal{F} = 3$ eV/Å. It is clear from the figure that the OQC results closely follow the elastica solutions for both the 3-element and 6-element models. The results also agree with beam theory solutions shown for the smallest values of the force $\mathcal{F}$. The small differences between the OQC and elastica solutions can be attributed to the fact that the elastica solution is limited to nonlinear kinematics with linear material, whereas OQC models nonlinear kinematics with a nonlinear material and also includes surface effects.

Next, to demonstrate the computational advantages of the OQC approach, we consider a nanobeam with a 1:100 side-to-length ratio. As before, the beam is fixed on the left and subjected to a vertical point load at its right end. The dimensions of the beam are $L_0 = 2400a_0 = 8676$ Å and $H = W = 24a_0 = 86.76$ Å for a total of 5 762 400 atoms in a fully atomistic simulation. This may be contrasted with the $6 \times 2401 = 14\,406$ atoms in all FDs of the OQC model.

The results for the nanobeam displacements for the applied forces $\mathcal{F} = 0.001$ eV/Å, 0.002 eV/Å, 0.003 eV/Å, and 0.004 eV/Å are illustrated in Fig. 9. As above, OQC results are shown in red and elastica results in blue. The OQC results agree very well for smaller loads. As the load increases, nonlinear material effects begin to be more pronounced in the OQC solution and the elastica model no longer provides an accurate solution for the problem.

This simulation provides an example for the advantages that OQC offers when approaching a very large system of atoms. A system such as this with over five million atoms is considered to be quite large for fully atomistic simulations and would require parallel computation with a large number of processors. In contrast, the OQC computations took just a few hours to run on a single 2.67-GHz Intel(R) Xeon (R) W3520 processor.

In all the OQC simulations described above, the FD consisted of 2401 atoms. This is a planar layer with a length (thickness) in the z direction of just $a_0 = 3.615$ Å. With an increase in the length of the FD, we expect to approach the results of fully atomistic simulations more closely. This is particularly important when loading the structure to the point where defects nucleate within the FD as incipient plasticity sets in. The importance of the FD size is demonstrated below.

B. Nanobeam deformed in pure bending

1. A [111]-oriented nanobeam

Consider a single-crystal copper nanobeam of length 957.99 Å with a square cross section of size 95.799 Å, i.e., with a side-to-length ratio of 1:10. The axis of the beam is in the [111] direction [see Fig. 7(c)] and $L_0 = 153a_z$, $H = W = 15.3a_z, a_z = \sqrt{3}a_0$. The system, fully simulated, consists

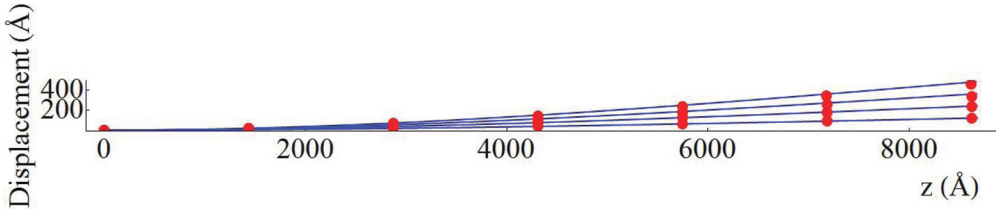

FIG. 9. (Color online) A nanobeam with a 1:100 side-to-length ratio is bent by the force applied to the right end, while keeping the left end fixed. A single-crystal copper nanobeam with square cross section of size $24a_0 = 86.76$ Å with a [100] nanobeam orientation is considered. The results of displacements are depicted for the applied force $\mathcal{F} = 0.001$ eV/Å, 0.002 eV/Å, 0.003 eV/Å, 0.004 eV/Å (from the bottom up). Data in red are for the OQC results (6 elements), and those in blue are for the elastica solution.

TABLE I. Elongation of a [111]-oriented nanobeam.

α (rad)	0.5	1.0	1.5	1.6
Elongation	0.042 %	0.17 %	0.34 %	3.07 %

of 740 061 atoms. We use an FD of 14 511 atoms, which corresponds to a slice of the nanobeam with a length of $3a_z$ in the initial undeformed state. The same EAM model for copper as in the previous simulations was used. The initial relaxation due to surface effects resulted in a change of length of 0.14%. As before, surface effect corrections[8] are not taken into account when comparing with the continuum results reported below. Since the nanobeam is subjected to pure bending, a single OQC element is sufficient to model the response.

The nanobeam is loaded by a pure moment $\mathcal{M}$ and as a result bends to an arc of angle $\alpha = \Delta\beta$ [see Fig. 4 and Eq. (7)]. [Note that for a single element with one end fixed ($\beta_1 = 0$), we have $\alpha = \beta_2$, i.e., α is the bending angle at the end of the beam.] The functional to minimize in this case is given in Eq. (16), with boundary conditions $z_1 = 0$ and $\beta_1 = 0$. Rather than applying the moment $\mathcal{M}$, it turns out to be computationally more efficient to apply the angle α as the boundary condition at the right end of the beam. ($\mathcal{M}$ and α are conjugate, so the two approaches are equivalent.) An incremental loading procedure with $\Delta\alpha = 0.05$ rad is adopted similar to that described above for the point load case. Our computations show that the [111]-oriented nanobeam experiences elongation as a result of the bending. Table I shows the change in total length of the nanobeam (relative to the initial relaxed undeformed length) when bent at an angle α.

The results for the bending moment versus bending angle are presented in Fig. 10. As we can see, for small angles, the relationship between $\mathcal{M}$ and α is linear and follows the beam theory prediction for bulk copper:

$$\mathcal{M} = \frac{Y I_z}{L_0}\alpha, \quad I_z = \frac{W H^3}{12}, \tag{24}$$

where Y stands for the appropriate directional Young's modulus in Eq. (23) and I_z is the area moment of inertia of the nanobeam with a square cross section about the z axis [see Fig. 7(a)]. Following the initial linear response, the bending moment softens a bit due to nonlinear effects until it reaches a critical value of $\alpha = 1.55$ rad (point 1 in Fig. 10) after which there is a discontinuous drop in both the moment and bending stiffness $k_b = \partial\mathcal{M}/\partial\alpha$. A linear response resumes at $\alpha = 1.6$ rad (point 2).

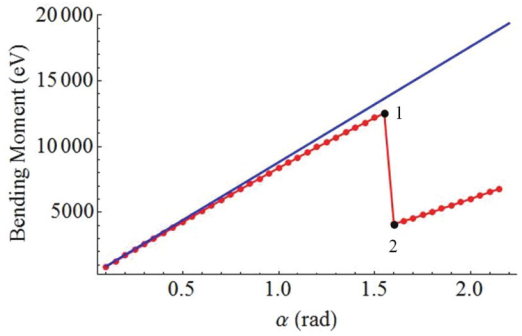

FIG. 10. (Color online) Bending moment $\mathcal{M}$ as a function of bending angle α for a [111]-oriented nanobeam with a length of 957.99 Å and a square cross section of side 95.799 Å. The blue line is the beam theory result in Eq. (24). Points 1 and 2 correspond to the state of the system just before and after a nucleation event in the FD. See text for explanation.

In order to understand the source of the discontinuity in the $\mathcal{M}$ versus α curve in Fig. 10, we investigate the atomic structure of the FD before and after the jump. To facilitate this, we compute the centrosymmetry parameter (CSP) for each of the atoms in the FD. The CSP is defined as follows:[32]

$$\text{CSP} = \sum_{i,1,6} \|\mathbf{R}_i + \mathbf{R}_{i+6}\|^2, \tag{25}$$

where $\mathbf{R}_i, \mathbf{R}_{i+6}$ correspond to six pairs of opposite nearest neighbors in the fcc lattice. The CSP is identically zero for centrosymmetric crystal structures (such as fcc and uniformly strained fcc) and has distinct values for particular defect structures as explained below.

Figure 11 shows the FD atoms just before [frames (a)–(c)] and just after [frames (d)–(f)] the discontinuous jump. The colors of atoms correspond to the values of the CSP parameter, with red representing atoms with $0 < \text{CSP} < 3$ which includes partial dislocations ($0.5 < \text{CSP} < 3$), light red to almost white representing stacking faults ($3 < \text{CSP} < 11$),

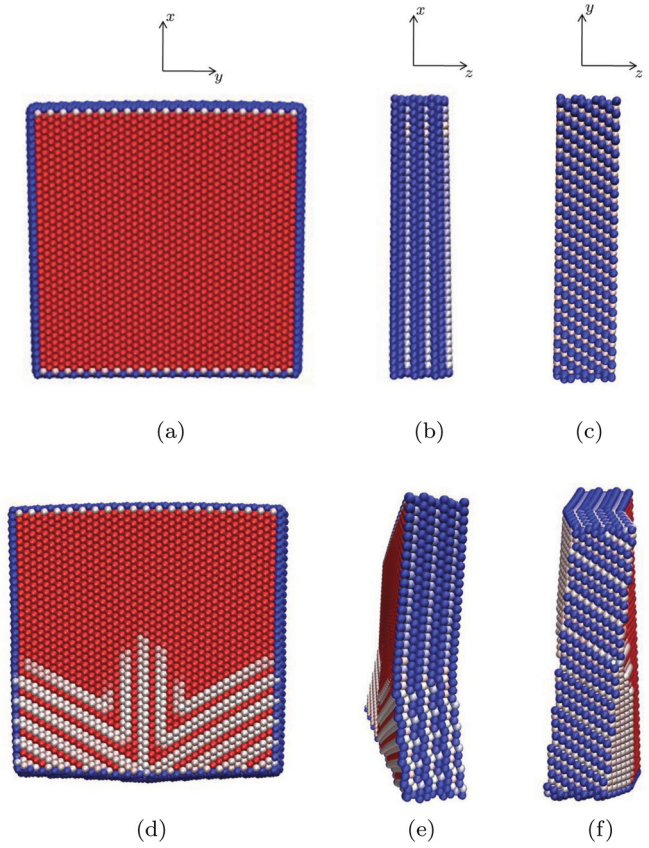

FIG. 11. (Color online) Defect structures in a FD of a [111]-oriented single-crystal copper nanobeam of size 95.799 Å by 957.99 Å: (a) front view of FD at $\alpha = 1.55$ rad, (b) side view, (c) bottom view; (d) front view of the FD at $\alpha = 1.6$ rad, (e) side view, (f) bottom view. The atoms are colored by CSP: $0 < \text{CSP} < 3$ (red), $3 < \text{CSP} < 11$ (light red to almost white), and $\text{CSP} > 11$ (light blue to blue). See text for explanation.

TABLE II. Contraction of [100]-oriented nanobeam.

α (rad.)	0.5	1.0	1.9	2.0
Contraction	0.097 %	0.39 %	1.64 %	4.44 %

light blue ($11 < \text{CSP} < 16$) are atoms either at or near the surface, and blue representing surface atoms ($\text{CSP} > 16$).[33] Clearly the discontinuous jump in the moment is associated with the nucleation of defects. The resulting structure consists of a series of stacking faults originating from the bottom (tension side) of this bent [111]-oriented nanobeam.

2. A [100]-oriented nanobeam

Consider next a [100]-oriented nanobeam of length 867.6 Å with a square cross section of size 86.76 Å. Thus, again the side-to-length ratio is 1:10. The system, when fully simulated, consists of 576 240 atoms and has a geometry of $L_0 = 240a_0$, $H = W = 24a_0$ where $a_0 = 3.615$ Å (see Fig. 7). The OQC model uses a FD of 7203 atoms which corresponds to a slice of the nanobeam of length $3a_0$ in the z direction. The initial relaxation in the FD due to surface effects is of magnitude 0.59%. As before, the beam is loaded in pure bending using an incremental procedure. Our computations show that the [100]-oriented nanobeam experiences contraction in total length when undergoing pure bending. Table II shows the change in the total length of the nanobeam (relative to the initial relaxed undeformed length) when bent to an angle α.

Figure 12(a) presents the bending moment versus bending angle response for the [100]- and [111]-oriented nanobeams. Both nanobeams (and all other cases considered below) have a 1:10 side-to-length ratio and are loaded up to a maximum strain of $\varepsilon_{\max} = 0.05\alpha$. [The maximum strain occurs at the upper and lower surfaces of the beam and is equal in magnitude to $\varepsilon_{\max} = H\alpha/(2L_0)$.] Note that the directional Young's modulus is different for the two nanobeams as defined in Eq. (23). Similar to the [111]-oriented nanobeam, the [100] beam experiences a sudden discontinuous drop in the bending moment. In this case, though, the stacking faults appear at the top (or compression side) of the beam [Fig. 12(b)], whereas for the [111] nanobeam [Fig. 12(c)], the stacking faults originate at the bottom (tension side).

3. Effect of the cross-section size

Consider again a [100]-oriented single-crystal copper nanobeam of length 867.6 Å. Two sets of simulations are compared: one with a cross-section size of $H = W = 24a_0$ (from above) and the other with $H = W = 18a_0$; for both cases, $H/L_0 = 1/10$ and the FD length is $3a_0$. The bending moment versus bending angle response for the two nanobeams are shown in Fig. 13. Interestingly, the discontinuities in the bending moment appear at the same critical angles [and hence the same critical strains ($\varepsilon_{\max}$)] for both nanobeams although the moment and bending stiffnesses vary.

4. Effect of the FD length

Finally, we consider the effect of changing the length of the FD in the z direction. This is interesting from a methodological standpoint since two OQC models with the same FD cross section and different lengths are ostensibly modeling the same beam. That means that any differences in the results reflect an artificial numerical constraint introduced by the objective boundary conditions inherent in OQC.

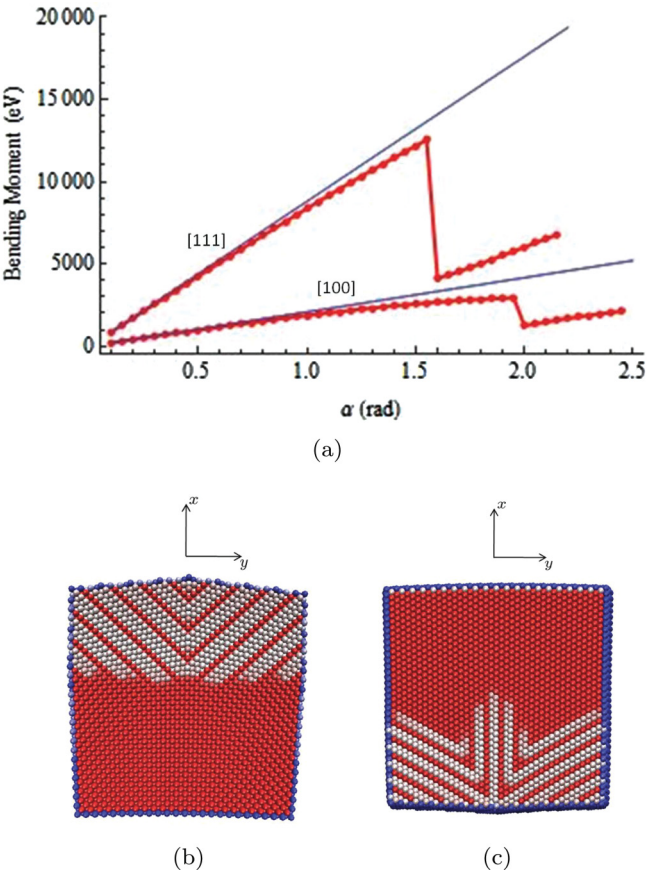

FIG. 12. (Color online) (a) Bending moment versus angle for nanobeams in pure bending for two orientations and sizes: a [100]-oriented nanobeam of size 86.76 Å by 867.6 Å; a [111]-oriented nanobeam of size 95.799 Å by 957.99 Å. The nanobeams are modeled with FDs of size $3a_0$ and $3a_z$, respectively. The OQC results (red) are compared with beam theory predictions (blue). (b) Defect structures for the [100]-oriented nanobeam with $\alpha = 2$ rad. (c) Defect structures for the [111] nanobeam with $\alpha = 1.6$ rad.

To explore this issue, we revisit the [100]-oriented nanobeam of size $H = W = 18a_0$ and $L_0 = 180a_0$, where

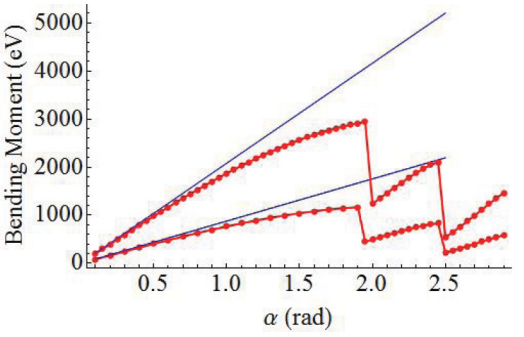

FIG. 13. (Color online) Bending moment $\mathcal{M}$ versus bending angle α for a [100]-oriented nanobeam with a side-to-length ratio of 1:10. The cross-section size is $24a_0$ for the upper curve and $18a_0$ for the lower curve.

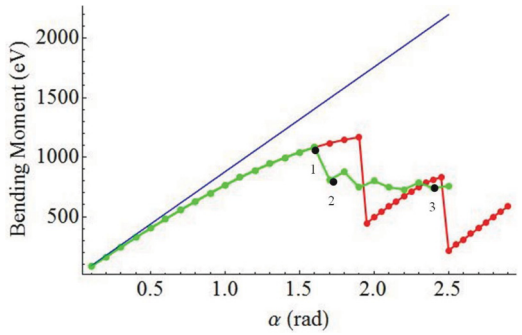

FIG. 14. (Color online) Bending moment $\mathcal{M}$ versus bending angle α for a [100]-oriented nanobeam with a side-to-length ratio of 1:10. The FD cross-section size is $18a_0$. The length of the FD is $3a_0$ for the red curve and $18a_0$ for the green curve. Points 1, 2, and 3 correspond to the angle values of 1.6, 1.7, and 2.4 rad.

$a_0 = 3.615$ Å. In Fig. 14, we compare the previous results obtained with a FD length of $3a_0$ to those obtained with a FD of length $18a_0$. As we can see, for angle values up to $\alpha = 1.5$ rad, both simulations produce the same results. With the shorter FD (of length $3a_0$), stacking faults first appear for larger values of the angle (or maximum strain). Evidently, the shorter FD imposes a mode of deformation with a very short repeat distance on the nanobeam.

In contrast, as seen in Fig. 15, a far more complex deformation mechanism is observed for the longer FD (of length $18a_0$). Three different states are shown: one at $\alpha = 1.6$ rad just before the appearance of the stacking faults [frames (a)–(c)] and two at $\alpha = 1.7$ and 2.4 rad after the initial nucleation event [frames (d)–(f) and frames (g)–(i)]. The very first defects nucleate at the top (or compression) side as observed for the shorter FD, however, the deformation after that takes on a

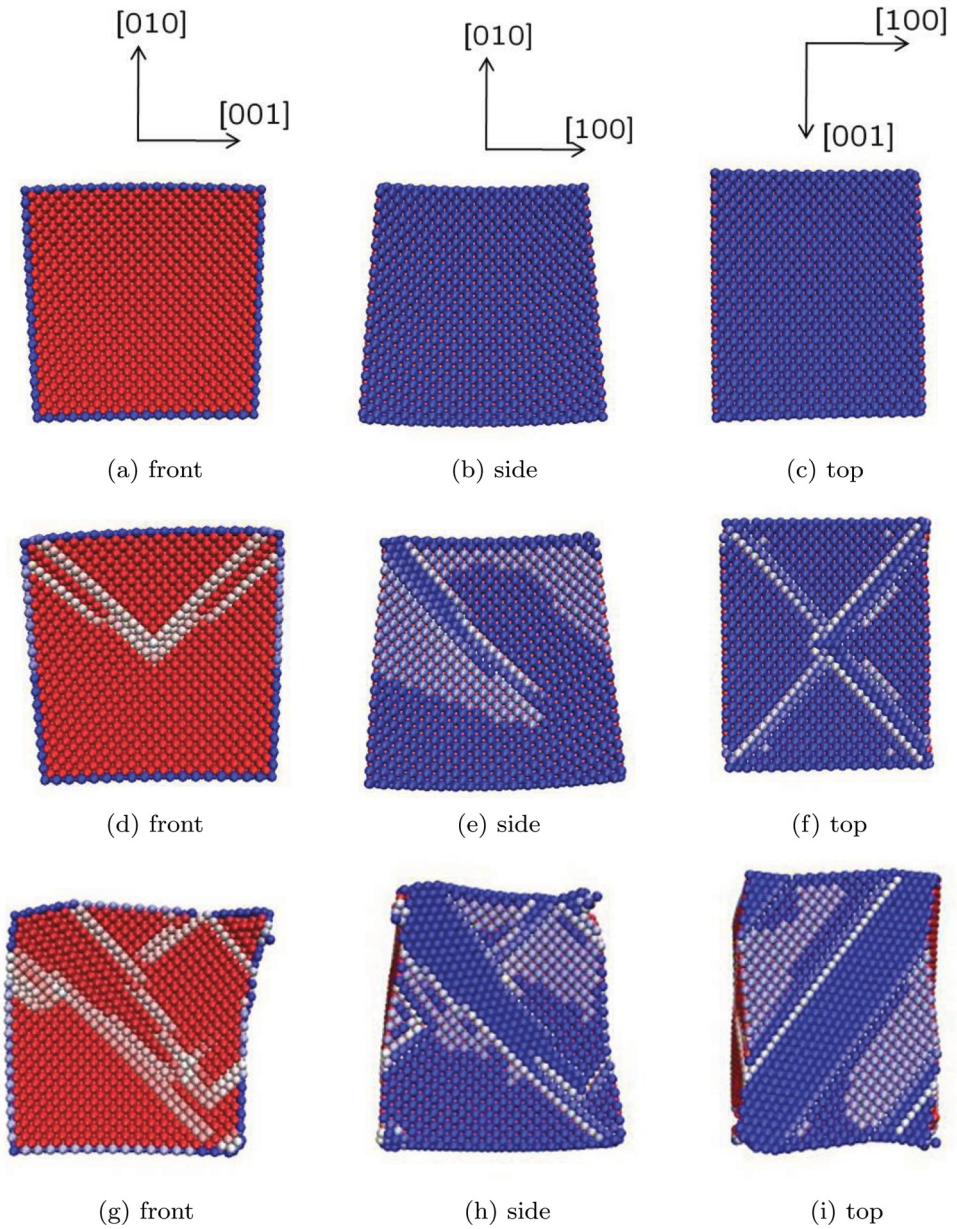

FIG. 15. (Color online) Dislocation structures for a [100]-oriented single-crystal copper nanobeam of length $180a_0$ and side $18a_0$, bent to an angle of $\alpha = 1.6$ rad for (a), (b), and (c); bent to $\alpha = 1.7$ rad for (d), (e), and (f); and bent to $\alpha = 2.4$ rad for (g), (h), and (i).

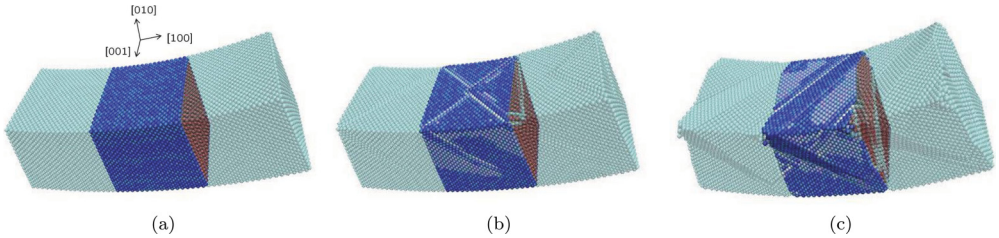

FIG. 16. (Color online) Deformed [100]-oriented nanobeam of cross-section side $18a_0$ and length $180a_0$. The FD (24642 atoms) of initial length $18a_0$ is shown together with image molecules on the left and right generated via objective boundary conditions at (a) $\alpha = 1.6$ rad, (b) $\alpha = 1.7$ rad, and (c) $\alpha = 2.4$ rad.

three-dimensional character. This is demonstrated in Fig. 16, which shows the entire FD (containing 24 642 atoms) with the image molecules generated by the objective boundary conditions.

Analyzing Figs. 12(b), 15, and 16, we see that in the [100]-oriented nanobeam the stacking faults and dislocations are formed on two primary planes: (111) and (11$\bar{1}$). As the bending angle is increased, the (111) plane becomes dominant as the defects on the (11$\bar{1}$) plane disappear [see Figs. 15(f) and 15(i)].

Another representation of the defect structure in the nanobeam is shown in Fig. 17 through the use of the dislocation extraction algorithm (DXA) described in Ref. 34. The DXA technique has been developed to find dislocations in atomistic simulation snapshots, to convert them to one-dimensional line segments, and to determine their Burgers vectors in a fully automated way. The method can be applied to complex dislocation processes in molecular dynamics simulations of some crystalline materials. In our case, a DXA analysis finds Shockley partial dislocations and stacking faults in the fcc lattice as shown in Fig. 17.

Figure 18 provides a closer look at dislocations and stacking faults in the FD with an angled view on the (100) plane [or see Fig. 15(d)] when $\alpha = 1.7$ and 2.4 rad. Partial dislocations

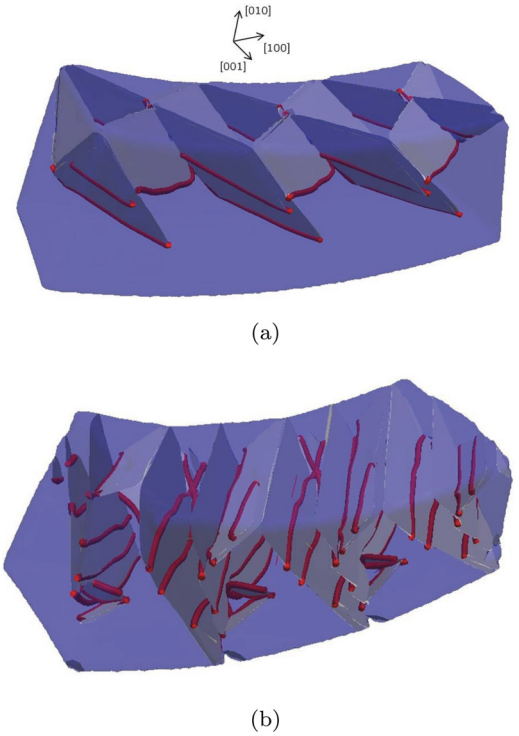

FIG. 17. (Color online) Deformed [100]-oriented nanobeam of cross-section side $18a_0$ and length $180a_0$. The FD (24 642 atoms) of initial length $18a_0$ is shown together with image molecules on the left and right generated via objective boundary conditions at (a) $\alpha = 1.7$ rad and (b) $\alpha = 2.4$ rad. Gray surfaces correspond to stacking faults and red tubes to dislocations.

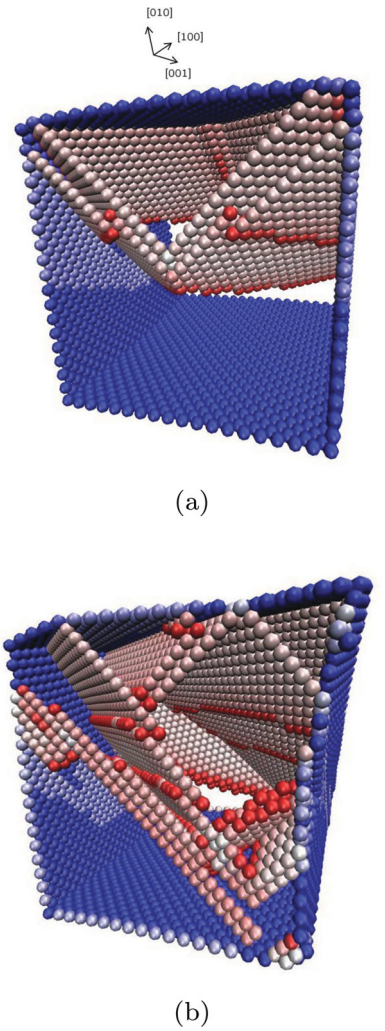

FIG. 18. (Color online) Deformed [100]-oriented nanobeam of cross-section side $18a_0$ and length $180a_0$. The FD (24 642 atoms) of initial length $18a_0$ is shown for (a) $\alpha = 1.7$ rad and (b) $\alpha = 2.4$ rad. Partial dislocations are red, stacking faults are light red to almost white, surface atoms are light blue to blue.

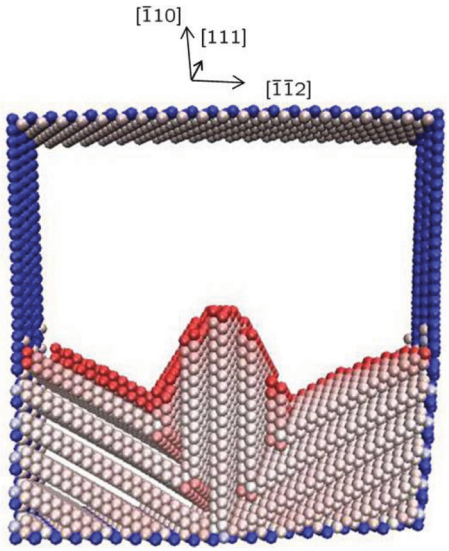

FIG. 19. (Color online) Defect structures in a FD of a [111]-oriented single-crystal copper nanobeam of size 95.799 Å by 957.99 Å, with $\alpha = 1.6$ rad as in Fig. 11(d). Partial dislocations are shown red, stacking faults are light red to almost white, surface atoms are light blue to blue.

are shown in red, stacking faults are light red to almost white, surface atoms are light blue to blue.

Figure 19 shows partial dislocations bounding stacking faults that nucleate on three major planes [($\bar{1}$11), (1$\bar{1}$1), and (11$\bar{1}$)] for the [111]-oriented nanobeam as in Fig. 11(d). A detailed analysis of the ($\bar{1}$11) [or (1$\bar{1}$1) due to symmetry] plane stacking faults reveals a polytypic structure. The term polytypic refers to structural modification due to the occurrence of stacking faults at regular intervals in crystals composed of close-packed layers of atoms. While the traditional notation for the layer sequence of closed-packed planes {111} in the fcc structure is $ABCABC\ldots$, the analysis of the ($\bar{1}$11) plane stacking faults shows a repeating sequence of nine layers: $ABCBCACAB$. In Ramsdell notation,[35] the structure is denoted as a 9R polytype, where the digit corresponds to the smallest number of repeated closed-packed layers (polytype cell size) and the letter specifies the lattice type (polytype cell symmetry): cubic "C," hexagonal "H," rhombohedral "R," etc. The occurrence of the polytype of the 9R type in Cu single crystals has been observed experimentally (see, for example, Refs. 36–40).

C. Error analysis

It is of interest to explore the accuracy of the OQC method and the convergence with respect to the number of elements.

A 1D OQC model consists of N elements delimited by $N+1$ nodes. The energy in each element is a function of the FD atoms and the symmetry parameters α_i and R_i ($i = 1,\ldots,N$) which are computed from the nodal degrees of freedom (see Sec. IV A). The symmetry parameters are constant within the element and discontinuous across element boundaries. It is expected that as the number of elements increases, this piecewise constant approximation to the exact nonuniform curvature will improve and OQC will converge to the correct result. To quantify this convergence, we apply an error estimator similar to the one used in the finite element method.[41,42]

To prevent having to deal with infinite radii of curvature, we choose to work in terms of the element bending angle α_i and curvature $c_i = 1/R_i$. Each of the $N+1$ nodes in the OQC model is assigned average values $\bar{\alpha}_i$ and $\bar{c}_i$ based on values in the neighboring elements with domains Ω_{i-1} and Ω_i:

$$\bar{\alpha}_i = \frac{\int \alpha_{i-1}\, d\Omega_{i-1} + \int \alpha_i\, d\Omega_i}{\int d\Omega_{i-1} + \int d\Omega_i}. \tag{26}$$

For the case of elements of the same size (also assumed below), we have

$$\begin{aligned} &\bar{\alpha}_i = (\alpha_{i-1} + \alpha_i)/2, \quad i = 2,\ldots,N \\ &\bar{\alpha}_1 = \alpha_1, \quad \bar{\alpha}_{N+1} = \alpha_N. \end{aligned} \tag{27}$$

Similarly,

$$\begin{aligned} &\bar{c}_i = (c_{i-1} + c_i)/2, \quad i = 2,\ldots,N \\ &\bar{c}_1 = c_1, \quad \bar{c}_{N+1} = c_N. \end{aligned} \tag{28}$$

Next, we construct an approximation for the element values $\hat{\alpha}_i$ and $\hat{c}_i$ from the *average* nodal values $\bar{\alpha}_i$ and $\bar{c}_i$ as follows:

$$\hat{\alpha}_i = (\bar{\alpha}_i + \bar{\alpha}_{i+1})/2, \quad \hat{c}_i = (\bar{c}_i + \bar{c}_{i+1})/2. \tag{29}$$

The error in element i, e_i, is now estimated by comparing the energy of the element with the one obtained using the approximated element variables:

$$e_i = \frac{E_i(\alpha_i, c_i) - E_i(\hat{\alpha}_i, \hat{c}_i)}{E_i(\alpha_i, c_i)}. \tag{30}$$

The error estimator used here is similar to the method introduced by Zienkiewicz and Zhu,[41] which can be used for any linear finite element discretization. While the methodology is not proven to work in all nonlinear problems, the numerical studies in Ref. 42 are encouraging.

We apply the error estimator in Eq. (30) to study the convergence of an OQC model for the fcc single-crystal copper nanobeam shown in Fig. 7. The nanobeam is of length $L_0 = 180a_0$ and $H = W = 6a_0$, where $a_0 = 3.615$ Å is the lattice constant of bulk fcc copper. The cantilever nanobeam is fixed at one end and loaded by a point force $\mathcal{F} = 0.006$ eV/Å at the other.

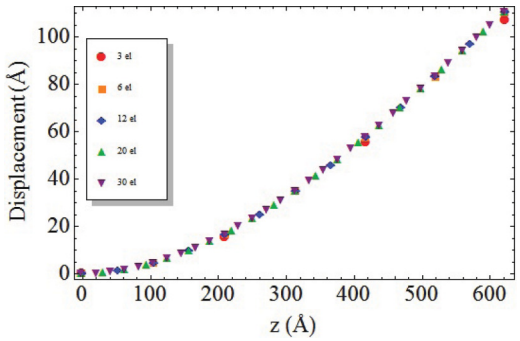

FIG. 20. (Color online) The nodal values of OQC results for nonuniform bending of single-crystal copper nanobeam, oriented in [100] direction. The point force $\mathcal{F} = 0.006/$ eV Åis acting at one end of the nanobeam of size $L_0 = 180a_0$ and $H = W = 6a_0$, while the other end is fixed.

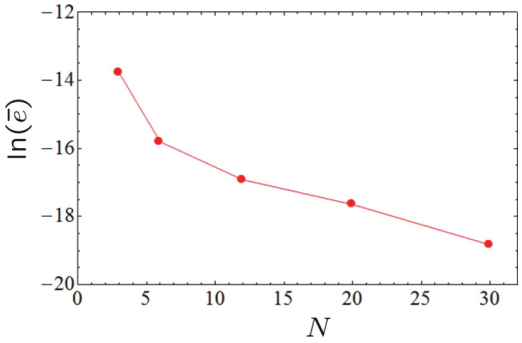

FIG. 21. (Color online) The average absolute error values (the natural logarithm is depicted) for different mesh refinements.

The nanobeam is modeled using $N = 3$, 6, 12, 20, and 30 OQC elements of equal size with a FD of length $3a_0$. The OQC results for each of these models are presented on Fig. 20. The computations appear to be quite accurate with the displacements from all models falling on a single curve. This is even true for the coarsest 3-element model. A more quantitative measure of the error is shown in Fig. 21, where the average absolute error

$$\bar{e} = \frac{1}{N}\sum_{i=1}^{N} |e_i| \tag{31}$$

is plotted as a function of the number of elements N on a semilog plot. The results indicate that the average error decreases with increasing mesh resolution.

VI. SUMMARY AND DISCUSSION

In this paper, we developed an objective quasicontinuum method for simulating rodlike structures that can be approximated locally as objective structures. This includes nanobeams, nanowires, nanotubes, viral parts, and various kinds of molecular fibers.

The OQC formulation is inspired by a Cosserat point element approach for nonlinear rods with rigid cross sections. In OQC, the rod is discretized into finite elements each of which is associated with a local OS through a set of symmetry parameters and a fundamental domain. The constitutive response within each element is obtained through an atomistic calculation where the positions of the atoms are defined through objective boundary conditions. This is a generalization of the Cauchy-Born approach to objective structures.

OQC has several advantages compared with fully atomistic and fully continuum approaches. First, OQC enjoys a computational advantage over fully atomistic methods such as molecular statics. This is because the number of degrees of freedom is reduced from $3N_{\text{atoms}}$ (where N_{atoms} is the total number of atoms in the structure) to about $3MN$ where M is the number of atoms in the fundamental domain and N is the number of elements (typically $MN \ll N_{\text{atoms}}$). In addition, the local OS calculations in each element are independent making the code easy to parallelize.

Second, unlike continuum rod theories in which the constitutive relations are phenomenological and therefore have a limited ability to predict new behavior, the constitutive response in OQC is atomistically based. The objective Cauchy-Born rule used in OQC naturally includes surface effects (important for nanostructures), nonlinear response at large deformation, failure mechanisms including dislocation nucleation and fracture at the FD level, and phase transformations. These complex behaviors are computed directly from the atomic interactions of the FD atoms and are only limited by the accuracy of the interatomic model. For ultimate accuracy, a first-principles approach such as density functional theory with objective boundary conditions could be used.[43]

As a test of the OQC formulation, it was applied to the bending of single-crystal copper nanobeams. The FD in this case is a slice of the nanobeam of a specified length. Two different cases were considered. The first test case was the nonuniform bending of a cantilever nanobeam loaded by a point force at its free end. For low values of the applied force, the results were in good agreement with elastica predictions using the directional Young's modulus computed from the interatomic potential. For larger values of the force, deviations between the OQC solution and elastica are observed which are mainly attributed to nonlinear material effects. The convergence of the OQC method with number of elements was studied using a finite element method based error estimator. The results show that the error for the nonuniform bending case is reduced as the number of elements is increased.

The OQC simulations for nonuniform bending were completed in a few hours on a single processor workstation. This reflects the efficiency of the OQC method which reduces the number of atoms that have to be simulated from about 5.7 million for the fully atomistic case to about 14 400 in the FDs of the OQC model.

Second, pure bending of a nanobeam was studied for two different crystallographic orientations with the beam axis along [100] and [111]. In both cases, the results agreed with the beam theory predictions for small values of the applied moment. As the magnitude of the loading is increased, some nonlinear softening is observed until a critical value is reached at which defects are nucleated within the FD. For the [100]-oriented nanobeam, a pattern of stacking faults is nucleated from the compressed side of the beam. For the [111] orientation, a similar pattern is observed to nucleate from the tension side of the beam.

The uniform bending results were repeated for a larger FD and found to be highly sensitive to the FD length. Instead of the planar stacking fault structures reported above, complex three-dimensional defect structures were observed. The selection of a suitable FD for a given problem is therefore an important question. One possibility is to run the simulation multiple times with increasing FD size until the desired output is seen to converge. This is similar to finite element simulations where convergence with respect to mesh size is the objective. Alternatively, one can adapt the FD size on-the-fly in order to meet certain accuracy requirements or when instabilities are detected. The latter approach, referred to as *cascading Cauchy-Born kinematics* (CCB), is used in multilattice QC simulations.[44] The adaption of CCB techniques to OQC is an interesting area for future research. Other areas for future OQC development include the extension to finite temperature as done in the so-called "hot-QC" method[45,46] and the inclusion of a *nonlocal* (i.e., atomistic) region as in the full QC method

in order to model isolated defects in otherwise objective structures.

ACKNOWLEDGMENTS

Authors acknowledge support of the National Science Foundation under Award No. DMS-0757355. This research was also partially supported by the National Science Foundation under the PIRE Grant No. OISE-0967140.

APPENDIX: FORCE COMPUTATION

In this section, we derive the forces acting on the atoms in the FD. For simplicity, let us first consider pair potential interactions between atoms i and j:

$$E_{ij} = \phi(r_{ij}), \quad r_{ij} = \|\mathbf{x}_i - \mathbf{x}_j\|, \tag{A1}$$

where $\mathbf{x}_i$ represents the coordinates of the ith atom. From the definitions above, it follows that

$$\frac{\partial r_{ij}}{\partial \mathbf{x}_k} = \frac{\mathbf{x}_i - \mathbf{x}_j}{r_{ij}} \frac{\partial(\mathbf{x}_i - \mathbf{x}_j)}{\partial \mathbf{x}_k}. \tag{A2}$$

For the case $i \in$ FD and $j \in$ FD, i.e., both atoms are in the fundamental domain, we have

$$\frac{\partial r_{ij}}{\partial \mathbf{x}_k} = \frac{\mathbf{x}_i - \mathbf{x}_j}{r_{ij}}(\delta_{ik} - \delta_{jk}), \qquad \delta_{ik} = \begin{cases} 1, & k = i \\ 0, & k \neq i. \end{cases} \tag{A3}$$

Thus, the pair interaction E_{ij} will contribute to the forces on atoms i and j:

$$-\frac{\partial E_{ij}}{\partial \mathbf{x}_k} = -\phi'(r_{ij})\frac{\mathbf{x}_i - \mathbf{x}_j}{r_{ij}}(\delta_{ik} - \delta_{jk}) = \begin{cases} \mathbf{f}_{ij}, & k = i \\ -\mathbf{f}_{ij}, & k = j \\ 0, & k \neq i, j \end{cases} \tag{A4}$$

where

$$\mathbf{f}_{ij} = -\phi'(r_{ij})\frac{\mathbf{x}_i - \mathbf{x}_j}{r_{ij}}. \tag{A5}$$

Now, consider the case where atom j is outside the FD and lies in one of the image molecules $J = -n_{\text{img}}, \ldots, -1, 1, \ldots, n_{\text{img}}$. Its position $\mathbf{x}_{J,j}$ is given by Eq. (9) which is repeated here for convenience:

$$\mathbf{x}_{J,j} = \mathbf{x}_c + \mathbf{Q}\left(\frac{\alpha J}{n_{\text{FD}}}\right) \cdot (\mathbf{x}_{\text{FD,j}} - \mathbf{x}_{\mathbf{c}}) + l_J \mathbf{Q}\left(\frac{\alpha J}{2n_{\text{FD}}}\right) \cdot \mathbf{d}, \tag{A6}$$

with $j = 1, \ldots, M$. We introduce the following notation for the force on atom i in the FD due to the presence of atom j in molecule J:

$$\mathbf{f}_{ij}^{(J)} \equiv \mathbf{f}(\mathbf{x}_i, \mathbf{x}_{J,j}) = -\phi'\left(r_{ij}^{(J)}\right)\frac{\mathbf{x}_{\text{FD,i}} - \mathbf{x}_{J,j}}{r_{ij}^{(J)}}. \tag{A7}$$

The subscript "FD" for $\mathbf{x}_i \in$ FD is dropped here and below for notational simplicity.

For the case where atoms $i,k \in$ FD, atom $j \notin$ FD, and all atoms have the same mass, using Eq. (A2) we obtain

$$-\frac{\partial E_{ij}^{(J)}}{\partial \mathbf{x}_k} = \begin{cases} \mathbf{f}_{ij}^{(J)} - \frac{1}{M}\left[\mathbf{I} - \mathbf{Q}\left(-\frac{\alpha J}{n_{\text{FD}}}\right)\right] \cdot \mathbf{f}_{ij}^{(J)}, & k = i \\ -\mathbf{Q}\left(-\frac{\alpha J}{n_{\text{FD}}}\right) \cdot \mathbf{f}_{ij}^{(J)} - \frac{1}{M}\left[\mathbf{I} - \mathbf{Q}\left(-\frac{\alpha J}{n_{\text{FD}}}\right)\right] \cdot \mathbf{f}_{ij}^{(J)}, & k = j \\ -\frac{1}{M}\left[I - \mathbf{Q}\left(-\frac{\alpha J}{n_{\text{FD}}}\right)\right] \cdot \mathbf{f}_{ij}^{(J)}, & \forall k \in \text{FD}, k \neq i, k \neq j \end{cases} \tag{A8}$$

where $\mathbf{I}$ is the identity matrix, M is the number of atoms in the FD. In the case of atoms with different masses, the term $1/M$ should be replaced by $m_k / \sum m_k$ where m_k is the mass of atom k. In the derivation of Eq. (A8), the orthogonality property of the matrices $\mathbf{Q}(\alpha)$ was used.

Taking into account that the positions of the *left* image atoms $J < 0$ are related to the positions of the *right* image atoms $J > 0$ [refer to Eqs. (A6) and (A7)], it is easy to derive the following connection between the force terms:

$$\mathbf{f}_{ij}^{(J<0)} = -\mathbf{Q}\left(-\frac{\alpha J}{n_{\text{FD}}}\right) \cdot \mathbf{f}_{ji}^{(J>0)} \quad \text{with} \quad \mathbf{f}_{ji}^{(J)} \equiv \mathbf{f}(\mathbf{x}_j, \mathbf{x}_{J,i}). \tag{A9}$$

From Eq. (A8) it follows that any atom $k \in$ FD is influenced by the pair interaction between atoms $i \in$ FD and $j \notin$ FD in the form of an additional contribution to its force:

$$-\frac{1}{M}\left[I - \mathbf{Q}\left(-\frac{\alpha J}{n_{\text{FD}}}\right)\right] \cdot \mathbf{f}_{ij}^{(J)}. \tag{A10}$$

The energy of the FD could be written as

$$E_{\text{FD}} = \sum_{i \in \text{FD}} \sum_{\substack{j \in \text{FD} \\ j > i}} E_{ij} + \frac{1}{2} \sum_{i \in \text{FD}} \sum_{\substack{j \notin \text{FD} \\ j \in (J>0)}} E_{ij} + \frac{1}{2} \sum_{i \in \text{FD}} \sum_{\substack{j \notin \text{FD} \\ j \in (J<0)}} E_{ij}. \tag{A11}$$

Using Eqs. (A4) and (A8)–(A11), we conclude that the total force on atom k in the FD can be written as

$$\mathbf{f}_{\text{FD,k}} = -\frac{\partial E_{\text{FD}}}{\partial \mathbf{x}_{\text{FD,k}}} = \sum_{\substack{j \in \text{FD} \\ j \neq k}} \mathbf{f}_{kj} + \frac{1}{2} \sum_{j \notin \text{FD}} \mathbf{f}_{kj}^{(J)} + \mathbf{f}_{\text{FD,k}}^{(\text{OS})}, \tag{A12}$$

where

$$\mathbf{f}_{\text{FD,k}}^{(\text{OS})} = -\frac{1}{M} \sum_{i \in \text{FD}} \sum_{j \notin \text{FD}} \left(\mathbf{f}_{ij}^{(J>0)} + \mathbf{f}_{ij}^{(J<0)}\right). \tag{A13}$$

Thus, in addition to usual summation of terms $\mathbf{f}_{kj}$ (used in periodic boundary conditions cases for example), there is an additional force term $\mathbf{f}^{(\mathrm{OS})}_{\mathrm{FD,k}}$ when objective boundary conditions are applied. The presence of this additional term is due to the symmetry of the OS, which is reflected in the objective boundary conditions specified in Eq. (9).

Equation (A12) is also correct for EAM potentials with the force term $\mathbf{f}_{kj}$ given in Eq. (A5) for a pair potential, replaced with the following EAM expression:

$$\mathbf{f}_{kj} = -[\phi'_{kj}(r_{kj}) + U'_k(\rho_k)g'_j(r_{kj}) + U'_j(\rho_j)g'_k(r_{kj})]\frac{\mathbf{x}_k - \mathbf{x}_j}{r_{kj}}. \tag{A14}$$

The force term in Eq. (A13) vanishes in the following cases: (1) under a state of axial loading where $\sum_{i\in\mathrm{FD}}\sum_{j\notin\mathrm{FD}}\mathbf{f}^{(J>0)}_{ij} = -\sum_{i\in\mathrm{FD}}\sum_{j\notin\mathrm{FD}}\mathbf{f}^{(J<0)}_{ij}$; and (2) in pure bending [Eq. (16)] with length of FD $> r_{\mathrm{cut}}$ ($>2r_{\mathrm{cut}}$ in case of EAM potential), where $\sum_{i\in\mathrm{FD}}\sum_{j\notin\mathrm{FD}}\mathbf{f}^{(J>0)}_{ij} = 0$ and therefore from Eq. (A9), also $\sum_{i\in\mathrm{FD}}\sum_{j\notin\mathrm{FD}}\mathbf{f}^{(J<0)}_{ij} = 0$. The proof of the statement (2) is as follows. Since the nanobeam is subjected to pure bending, a single OQC element is sufficient to model the response and the total potential energy follows from Eq. (14) as

$$\Pi = E_{\mathrm{FD}}(z_1,\beta_1,z_2,\beta_2,\{\mathbf{x}_{\mathrm{FD,k}}\}_{k=1,\ldots,M}) - \mathcal{M}\beta_2. \tag{A15}$$

Following the derivation above and using Eqs. (A11) and (A6), we arrive at

$$\begin{aligned}\frac{\partial E_{\mathrm{FD}}}{\partial z_p} &= \sum_{i\in\mathrm{FD}}\sum_{j\notin\mathrm{FD}}\frac{\partial E_{ij}}{\partial z_p}\\ &= \sum_{i\in\mathrm{FD}}\sum_{j\notin\mathrm{FD}}\frac{\partial l_J}{\partial z_p}\mathbf{Q}\left(-\frac{\alpha J}{2n_{\mathrm{FD}}}\right)\cdot\mathbf{f}^{(J)}_{ij}, \quad p = 1,2\end{aligned} \tag{A16}$$

where $\alpha = \beta_2 - \beta_1$, and from Eqs. (10) and (8) we have

$$\frac{\partial l_J}{\partial z_p} = \frac{\partial L}{\partial z_p}\frac{\sin\frac{\alpha J}{2n_{\mathrm{FD}}}}{\sin\frac{\alpha}{2}}. \tag{A17}$$

Substituting this into Eq. (A16) and separating the sum into contributions for $J > 0$ and $J < 0$, we obtain

$$\begin{aligned}\frac{\partial E_{\mathrm{FD}}}{\partial z_p} = \frac{\partial L}{\partial z_p}\sum_{i\in\mathrm{FD}}\Bigg(&\sum_{j\notin\mathrm{FD}}\frac{\sin\frac{\alpha|J|}{2n_{\mathrm{FD}}}}{\sin\frac{\alpha}{2}}\mathbf{Q}\left(-\frac{\alpha|J|}{2n_{\mathrm{FD}}}\right)\cdot\mathbf{f}^{(J>0)}_{ij}\\ &- \sum_{j\notin\mathrm{FD}}\frac{\sin\frac{\alpha|J|}{2n_{\mathrm{FD}}}}{\sin\frac{\alpha}{2}}\mathbf{Q}\left(\frac{\alpha|J|}{2n_{\mathrm{FD}}}\right)\cdot\mathbf{f}^{(J<0)}_{ij}\Bigg).\end{aligned} \tag{A18}$$

Next, using the connection between the force terms in Eq. (A9), we finally arrive at

$$\frac{\partial E_{\mathrm{FD}}}{\partial z_p} = 2\frac{\partial L}{\partial z_p}\sum_{i\in\mathrm{FD}}\sum_{j\notin\mathrm{FD}}\frac{\sin\frac{\alpha J}{2n_{\mathrm{FD}}}}{\sin\frac{\alpha}{2}}\mathbf{Q}\left(-\frac{\alpha J}{2n_{\mathrm{FD}}}\right)\cdot\mathbf{f}^{(J>0)}_{ij}. \tag{A19}$$

Thus, due to the energy minimization condition in Eq. (21) and noting that for the case of pure bending $\partial W/\partial z_p = 0$, we have

$$\frac{\partial E_{\mathrm{FD}}}{\partial z_p} = 2\frac{\partial L}{\partial z_p}\sum_{j\notin\mathrm{FD}}\frac{\sin\frac{\alpha J}{2n_{\mathrm{FD}}}}{\sin\frac{\alpha}{2}}\mathbf{Q}\left(-\frac{\alpha J}{2n_{\mathrm{FD}}}\right)\cdot\sum_{i\in\mathrm{FD}}\mathbf{f}^{(J>0)}_{ij} = 0. \tag{A20}$$

For the case where $J = 1$, i.e., the length of the FD is more than r_{cut} (or $2r_{\mathrm{cut}}$ in case of an EAM potential), which is a common choice in computations (including the pure bending computations performed here), we have

$$\sum_{i\in\mathrm{FD}}\sum_{j\notin\mathrm{FD}}\mathbf{f}^{(J>0)}_{ij} = 0, \tag{A21}$$

and thus from (A9) also

$$\sum_{i\in\mathrm{FD}}\sum_{j\notin\mathrm{FD}}\mathbf{f}^{(J<0)}_{ij} = 0. \tag{A22}$$

Referring to the above two equations, we see from Eq. (A13) that

$$\mathbf{f}^{(\mathrm{OS})}_{\mathrm{FD,k}} = 0, \tag{A23}$$

which proves statement (2).

*yh77@cornell.edu
†tadmor@aem.umn.edu
‡james@aem.umn.edu

[1] E. W. Wong, P. E. Sheehan, and C. M. Lieber, Science **277**, 1971 (1997).
[2] M. M. J. Treacy, T. W. Ebbesen, and J. M. Gibson, Nature (London) **381**, 678 (1996).
[3] J.-P. Salvetat, J.-M. Bonard, N. H. Thomson, A. J. Kulik, L. Forró, W. Benoit, and L. Zuppiroli, Appl. Phys. A **69**, 255 (1999).
[4] A. N. Cleland and M. L. Roukesi, Appl. Phys. Lett. **69**, 2653 (1996).
[5] N. Osakabe, K. Harada, M. I. Lutwyche, H. Kasai, and A. Tonomura, Appl. Phys. Lett. **70**, 940 (1997).
[6] C. M. Lieber, MRS Bull. **28**, 486 (2003).
[7] P. Yang, MRS Bull. **30**, 85 (2005).
[8] R. E. Miller and V. B. Shenoy, Nanotechnology **11**, 139 (2000).
[9] B. Bar On, E. Altus, and E. B. Tadmor, Int. J. Solids Struct. **47**, 1243 (2010).
[10] D. E. Segall, S. Ismail-Beigi, and T. A. Arias, Phys. Rev. B **65**, 214109 (2002).
[11] E. B. Tadmor, M. Ortiz, and R. Phillips, Philos. Mag. A **73**, 1529 (1996).
[12] V. B. Shenoy, R. Miller, E. Tadmor, D. Rodney, R. Phillips, and M. Ortiz, J. Mech. Phys. Solids **47**, 611 (1999).
[13] E. B. Tadmor, G. S. Smith, N. Bernstein, and E. Kaxiras, Phys. Rev. B **59**, 235 (1999).
[14] M. B. Rubin, *Cosserat Theories: Shells, Rods and Points*, Vol. 79 of Solid Mechanics and its Applications (Kluwer, Dordrecht, The Netherlands, 2000).
[15] M. Brand and M. B. Rubin, Int. J. Nonlinear Mech. **42**, 216 (2007).
[16] T. Dumitrica and R. D. James, J. Mech. Phys. Solids **55**, 2206 (2007).

[17]R. D. James, J. Mech. Phys. Solids **54**, 2354 (2006).
[18]A. E. H. Love, *A Treatise on the Mathematical Theory of Elasticity*, 4th ed. (Dover, New York, 1994).
[19]S. S. Antman, *The Theory of Rods* (Springer, Berlin, 1972), Vol. VIa/2.
[20]S. S. Antman, *Nonlinear Problems of Elasticity*, 2nd ed. (Springer, New York, 2005).
[21]A. E. Green, P. M. Naghdi, and M. L. Wenner, Proc. R. Soc. London **A337**, 451 (1974).
[22]A. E. Green, P. M. Naghdi, and M. L. Wenner, Proc. R. Soc. London **A337**, 485 (1974).
[23]M. B. Rubin, Int. J. Solids Struct. **38**, 4395 (2001).
[24]M. B. Rubin, J. Appl. Mech. **52**, 368 (1985).
[25]B. Nadler and M. B. Rubin, Int. J. Solids Struct. **40**, 4584 (2003).
[26]E. B. Tadmor and R. E. Miller, *Modeling Materials: Continuum, Atomistic and Multiscale Techniques* (Cambridge University Press, Cambridge, UK, 2011).
[27]M. S. Daw and M. I. Baskes, Phys. Rev. B **29**, 6443 (1984).
[28]N. C. Admal and E. B. Tadmor, J. Elasticity **100**, 63 (2010).
[29]S. M. Foiles, M. I. Baskes, and M. S. Daw, Phys. Rev. B **33**, 7983 (1986).
[30]L. D. Landau and E. M. Lifshitz, *Theory of Elasticity*, 3rd ed. (Pergamon, New York, 1986).
[31]J. F. Nye, *Physical Propertis of Crystals: Their Representation by Tensors and Matrices* (Oxford University Press, London, UK, 1957).
[32]C. L. Kelchner, S. J. Plimpton, and J. C. Hamilton, Phys. Rev. B **58**, 11085 (1998).
[33]K. Zhao and C. Chen, *Advances in Heterogeneous Material Mechanics Proceedings* (DEStech Publications, Lancaster, PA, 2008), pp. 338–341.
[34]A. Stukowski and K. Albe, Model. Simul. Mater. Sci. Eng. **18**, 085001 (2010).
[35]G. C. Trigunayat, Solid State Ionics **48**, 3 (1991).
[36]P. J. Othen, M. L. Jenkins, G. D. W. Smith, and W. J. Phythian, Philos. Mag. Lett. **64**, 383 (1991).
[37]F. Ernst, M. W. Finnis, A. Koch, C. Schmidt, B. Straumal, and W. Gust, Z. Metall. **87**, 911 (1996).
[38]J. J. Blackstock and G. J. Ackland, Philos. Mag. A **81**, 2127 (2001).
[39]S. Dymek and M. Wrobel, Mater. Chem. Phys. **81**, 552 (2003).
[40]J. Chen, W. Yan, and X.-H. Fan, Trans. Nonferrous Met. Soc. China **19**, 108 (2009).
[41]O. C. Zienkiewicz and J. Z. Zhu, Int. J. Numer. Methods Eng. **24**, 337 (1987).
[42]T. Belytschko and M. Tabbara, Int. J. Numer. Methods Eng. **36**, 4245 (1993).
[43]A. S. Banerjee, M.S. thesis, University of Minnesota, 2011.
[44]M. Dobson, R. S. Elliott, M. Luskin, and E. B. Tadmor, J. Comput.-Aided Mater. Des. **14**, 219 (2007).
[45]L. M. Dupuy, E. B. Tadmor, R. E. Miller, and R. Phillips, Phys. Rev. Lett. **95**, 060202 (2005).
[46]E. B. Tadmor, F. Legoll, W. K. Kim, L. M. Dupuy, and R. E. Miller (unpublished).